Journal of Photochemistry and Photobiology A: Chemistry 222 (2011) 351–359

Contents lists available at ScienceDirect

Journal of Photochemistry and Photobiology A: Chemistry

journal homepage: www.elsevier.com/locate/jphotochem

Europium hybrids/SiO_2/semiconductor: Multi-component sol–gel composition, characterization and photoluminescence

Bing Yan*, Yan Zhao, Qiu-Ping Li

Department of Chemistry, Tongji University, Siping Road 1239, Shanghai 200092, China

ARTICLE INFO

Article history:
Received 29 April 2011
Received in revised form 4 July 2011
Accepted 15 July 2011
Available online 23 July 2011

Keywords:
Hybrids or composite
Europium complex
Luminescent property
Metal sulfide

ABSTRACT

Three kinds of semiconductor metal sulfide nanoparticles (CdS, ZnS, Ag_2S) are synthesized and then are functionalized with 3-mercaptopropyltrimethoxysilane (MPTMS) to obtain organically modified MPTMS–CdS(ZnS, Ag_2S) composite. Meanwhile, ternary europium complex systems are synthesized with trifluoroacetylacetone (TAA) functionalized linkage (TAASi) and terminal N-heterocyclic ligand (Phen = 1,10-phenanthroline, Bipy = 2,2′-bipyridyl). Then through the co-hydrolysis and copolycondensation processes between TTASi unit of Phen(Bipy)-Eu-TAASi and MPTMS unit of MPTMS/CdS(ZnS, Ag_2S), both of the semiconductor unit and rare earth complex system are sol–gel composed with covalently bonding Si–O to form the multi-component inorganic/organic hybrids Phen(Bipy)-Eu-TAASi–SiO_2–MPTMS–CdS(ZnS, Ag_2S). The luminescent properties of these hybrids are studied in detail, which shows the introduction of semiconductor unit is favorable for the luminescence of europium ions.

1. Introduction

Trivalent rare earth ions have excellent luminescent properties in the visible and near-infrared regions such as large Stokes shifts, high luminescence quantum efficiency, and line-like emission spectra, which make them applied in all kinds of practical fields such as phosphors, devices and biological images [1–3]. Unfortunately, rare earth ions themselves have not been widely and directly applied to luminescent materials for low molar absorption coefficients aroused by spin-forbidden f–f transitions and inefficient direct photoexcitation. In order to improve the luminescence of rare earth ions, two paths are utilized with the ionic or atomic type and molecular type. The ionic or atomic type is to dope the photoactive RE^{3+} into the special matrices such as all kinds oxides and oxysalts, which has been extensively investigated for the phosphors [4–6]. The molecular type is to design rare earth complexes comprising sensitizing ligands such as β-diketones, aromatic carboxylic acids and heterocyclic ligands due to their excellent coordination ability and proper energy level match. But these molecular systems still exist with poor stability for practical applications [7,8]. To overcome the disadvantages, rare earth complexes can also be fabricated into inorganic matrices as photoactive species to integrate the photophysical properties of the organic component and the favorable thermal and mechanical characters of the inorganic networks simultaneously [9,10]. At present most of the works are focused on the chemical bonding between the rare earth complex species and the inorganic matrix through unique functional molecular bridge [11–15]. In nature, these hybrids embody the features of not only rare earth doped phosphors but also rare earth complexes because the organically functionalized Si–O component can behave as both host and ligand, and the luminescence of them can be enhanced remarkably. However, these hybrids generally belong to amorphous non-crystalline materials, whose exact characterization of composition and structure is difficult and limits the application in the practical fields. So it is necessary to introduce crystalline unit to assemble the novel hybrid material.

On the other hand, semiconductor materials including III–V group or II–VI group compounds are another type of important luminescent materials for opto-electronic application [16,17], especially LED display or lighting devices, whose luminescent principle is different from rare earth ions and can be integrated with rare earth ions to realize the white emission for device [18,19]. In the recent years, there are considerable investigations on the semiconductor doped with rare earth ions [20–28]. But the most of these doping systems mainly show the luminescence of rare earth ions, which do not show any advantage compared to the individual units. All kinds of semiconductor species are doped with rare earth ions, such as III–V group (GaN, AlGaN, AlInN etc.) [20–22] and II–VI group (TiO_2, ZnO, ZnS etc.) [23–26]. For example, study of the luminescence of rare earth ions introduced into III-nitride semiconductor hosts produces a wealth of important information of photoluminescence and cathodoluminescence spectroscopy with hosts including

* Corresponding author. Tel.: +86 21 65984663; fax: +86 21 65982287.
E-mail address: byan@tongji.edu.cn (B. Yan).

1010-6030/$ – see front matter © 2011 Elsevier B.V. All rights reserved.
doi:10.1016/j.jphotochem.2011.07.010

GaN, AlGaN and AlInN [24]. Besides, the surface modification of semiconductor nanoparticles is easy to prepare the all kinds of functional composites [29,30], but a few works can be paid attention on the multi-component assembly between semiconductor and rare earth complexes with covalent linkage [31,32].

In this paper, we provide another strategy to realize the composing of the versatile multi-component hybrid material systems that consist of photoactive rare earth unit and functionalized semiconductor unit through the covalent bonds. Firstly semiconductor metallic sulfides are prepared and modified with mecapto silane (3-mercaptopropyltrimethoxysilane (MPTMS). Secondly, rare earth complex system of the covalenty linkage are then chemically bonded with above functionalized semiconductor through sol-gel process. The detailed characterization and especially the photoluminescent properties of these hybrids are investigated, which can provide interesting data for the novel photofunctional rare earth semiconductor hybrid materials.

2. Experimental

2.1. Materials

Cadmium chloride ($CdCl_2{\cdot}2.5H_2O$), sodium sulfide ($Na_2S{\cdot}9H_2O$) and silver nitrate ($AgNO_3$) are supplied by Sinopharm chemical reagent. Zinc acetate dehydrate ($Zn(AC)_2{\cdot}2H_2O$) and ethanethioamide (H_3CCSNH_2) are obtained from Shanghai Chemical Plant. 3-(Triethoxysilyl)-propyl isocyanate (TESPIC), 3-mercaptopropyltrimethoxysilane (MPTMS), sodium thiosulfate ($Na_2S_2O_3{\cdot}5H_2O$) and trifluoroacetylacetone (TAA) are purchased from Aldrich. The modified precursor TAASi is synthesized using a procedure previously [33]. Europium nitrate is obtained by dissolving Eu_2O_3 in concentrated nitric acid. Tetraethoxysilane (TEOS, Aldrich) is distilled and stored under nitrogen atmosphere. The solvent tetrahydrofuran (THF) is used after desiccation process by anhydrous calcium chloride. All the other reagents are analytically pure.

2.2. Synthesis of CdS nanorods

The CdS nanorods are synthesized by dissolving 1 mmol cadmium chloride ($CdCl_2{\cdot}2.5H_2O$) in 40 mL H_2O with constant stirring. To this, 1 mmol $Na_2S_2O_3{\cdot}5H_2O$ is added while stirring. The stirring is continued for another 30 min to yield a colorless solution; the reaction mixture is added into a closed reactor (with Teflon inside) at 120 °C for 6 h. The orange precipitate is centrifuged and then washed twice with acetone and twice with ethanol. All the samples are dried at 60 °C for 12 h in a vacuum oven.

2.3. Synthesis of ZnS nanoparticles

The precipitation of ZnS nanoparticles is performed from homogeneous solutions of zinc acetate [$Zn(CH_3COO)_2{\cdot}2H_2O$] at 0.3 M and thioacetamide (H_3CCSNH_2) at 0.3 mol L^{-1} for each precipitation reaction. The reaction temperature is fixed at 80 °C. The solution containing H_3CCSNH_2 is poured into the zinc acetate solution under vigorous stirring for several minutes, and white colloids are formed immediately. The precipitated ZnS nanoparticles are washed twice with water and twice with isopropyl alcohol. Then, the supernatant is removed by centrifugation, and the ZnS nanoparticles are obtained by drying the precipitation at room temperature for about 12 h in a vacuum oven.

2.4. Synthesis of Ag_2S nanoparticles

Silver nitrate in water (10 mL of 0.1 mol L^{-1}) is mixed with 20 mL of 0.1 mol L^{-1} $Na_2S{\cdot}9H_2O$ solution while vigorous stirring. The obtained black precipitate of silver sulfide is centrifuged and then washed twice with water and twice with ethanol. The Ag_2S nanoparticles are subsequently dried at 60 °C for 12 h in a vacuum oven.

2.5. Synthesis of MPTMS–CdS(MPTMS–ZnS, MPTMS–Ag_2S)

1 mmol, CdS nanorods (ZnS, Ag_2S) are dissolved in 30 mL of ethanol under stirring. After the mixtures are stirred for 30 min, 0.247 g of MPTMS is added and then reacted for about 1 h at room temperature under vigorous stirring. Finally, the resulting (MPTMS–CdS(ZnS, Ag_2S)) nanoparticles are obtained by centrifugation.

2.6. Synthesis of the hybrid materials Phen-Eu-TAASi–SiO_2–MPTMS–CdS(ZnS, Ag_2S)

While being stirred, the precursor TAASi (3 mmol) is dissolved in DMF solution, 1 mmol $Eu(NO_3){\cdot}6H_2O$ and Phen are added. After 3 h, 3 mmol MPTMS–CdS(ZnS, Ag_2S) is added. After the treatment of hydrolysis for 6 h, an appropriate amount of hexamethylenetetramine is added to adjust the pH value to 6–7. The resulting mixture is agitated magnetically to achieve a single phase, and thermal treatment is performed at 70 °C in a covered Teflon beaker for several days until the sample solidified.

2.7. Synthesis of the hybrid materials Bipy-Eu-TAASi–SiO_2–MPTMS–CdS(ZnS, Ag_2S)

While being stirred, the precursor TAASi (3 mmol) is dissolved in DMF solution, 1 mmol $Eu(NO_3){\cdot}6H_2O$ and Bipy are added. After 3 h, 3 mmol MPTMS–CdS(MPTMS–ZnS and MPTMS–Ag_2S) is added. After the treatment of hydrolysis for 6 h, an appropriate amount of hexamethylenetetramine is added to adjust the pH value to 6–7. The resulting mixture is agitated magnetically to achieve a single phase, and thermal treatment is performed at 70 °C in a covered Teflon beaker for several days until the sample solidified.

2.8. Physical measurements

The X-ray powder diffraction patterns are recorded on a Bruker D8 diffractometer (40 mA–40 kV) using monochromated CuKα1 radiation (k) (λ = 1.5406 Å) over the 2θ range of 10–70°. FT-IR spectra are obtained within the 4000–400 cm^{-1} region on an infrared spectrophotometer with the KBr pellet technique. The ultraviolet–visible diffuse reflectance is acquired by a BWS003 spectrophotometer. The microstructure is estimated by scanning electronic microscope (SEM; Philips XL-30). Ultraviolet absorption spectra of these powder samples (5×10^{-4} mol L^{-1} chloroform ($CHCl_3$) solution) were recorded with an Agilent 8453 spectrophotometer. The luminescence excitation and emission spectra are obtained by a RF-5301 spectrophotometer. Luminescence lifetime measurements are carried out on an Edinburgh FLS920 phosphorimeter using a 450 W xenon lamp as the excitation source. All the emission spectra are corrected and the intensities are determined with integrated area. All measurements are performed at room temperature.

3. Results and discussion

Fig. 1 shows the scheme for the synthesis process and major composition in the whole hybrid systems, which involves three complicated units: metal sulfide composite, organically modified silica hybrids from double siliane linkage (MPTMS and TESPIC) and rare earth complex system, respectively. Firstly, three metal sulfide composite can be prepared by the modification between

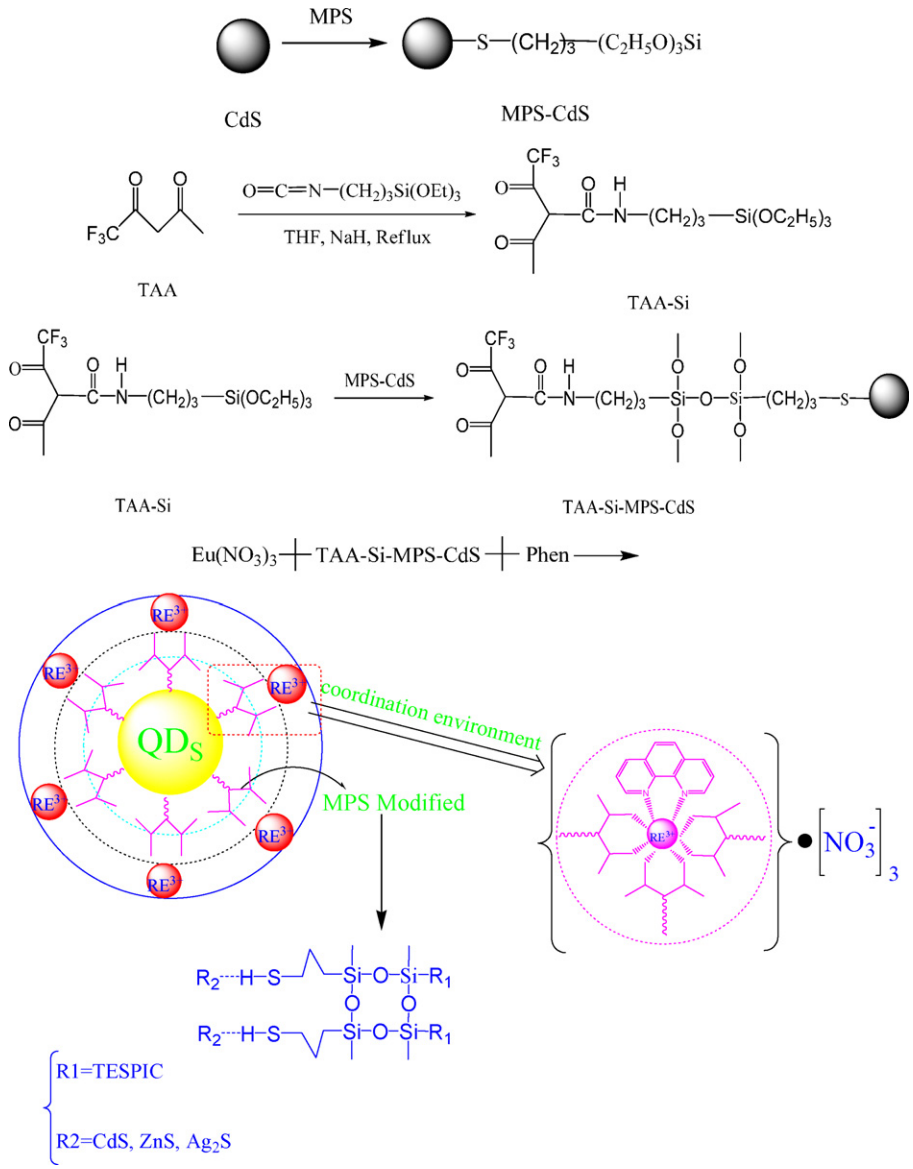

Fig. 1. The selected scheme for the **s**ynthesis process and predicted structure of the hybrids Phen-Eu-TAA–Si–MPTMS–CdS.

mecapto group of MPTMS siloxane and their nanoparticle for the chemical affinity between transition metal ions (CdS, ZnS, Ag_2S as soft base) and S atoms of mecapto group of MPTMS (as soft acid). Then europium ion is coordinated to TTASi linkage through its chelated carbonyl group oxygen atoms and Phen (or Bipy) as assistant ligands through the two chelated nitrogen atoms. So eight-coordination position surrounding Eu^{3+} is filled and close to the common coordination number of Eu^{3+} according to rare earth chemistry principle. Besides, three nitrate ions are located surrounding the Eu^{3+} to behave as counter anions. Finally, the multi-component hybrid system is assembled through the Si–O covalently bonds by the cohydrolysis and copolycondensation processes between MPTMS–CdS(ZnS,Ag_2S) unit and Phen(Bipy)-Eu-TAASi unit. In nature, the whole hybrid system is assembled through the double cross-linking siloxane to form the covalent bonding between Eu complex and modified metal sulfide nanoparticles.

Fig. 2 shows the FT-IR spectra of three semiconductor metal sulfides and their multicomponent hybrids with photoactive rare earth systems (Phen(Bipy)-Eu-TTASi–SiO_2–MPTMS–CdS(ZnS, Ag_2S) are shown in Fig. 2. For Fig. 2(a) for CdS-based systems, the 1621 and 3430 cm^{-1} are corresponded to bending vibration and unsymmetrical stretching vibration absorption peaks of the H_2O molecules (mainly surface adsorbed H_2O). No Cd–O stretching vibration peak can be found in the low frequency of 420–460 cm^{-1}. This suggests that no oxidation phenomenon occurs and CdS is stable. The IR spectra of Phen(Bipy)-Eu-TTASi–SiO_2–MPTMS–CdS material are similar for the similar multicomponent hybrid systems except for the difference of Phen and Bipy. The vibration of $-CH_2-$ at 3065 cm^{-1} is replaced by a strong broad band at 2920 cm^{-1}, which is originated from the methylene groups of TESPIC [34]. Moreover, the disappearance of the stretching vibration of the absorption peaks located at 2250–2275 cm^{-1} for N=C=O of TESPIC indicate that TESPIC has completely taken part in the grafting reaction with the organic compound MPTMS. Besides, the absorption bands at 1023 to 1130 cm^{-1} due to the vibration of Si–O–Si can be detected, indicating the formation of Si–O during the hydrolysis and polycondensation processes. The wide band absorption at the range of 3000–3700 cm^{-1} can be ascribed the overlap of the asymmetric and symmetric stretches (H–O–H) in the crystallized water (3600–3000 cm^{-1}), and N–H (3500–3200 cm^{-1}) in TESPIC. No absorption bands ranged in 2600–2550 cm^{-1} can be observed

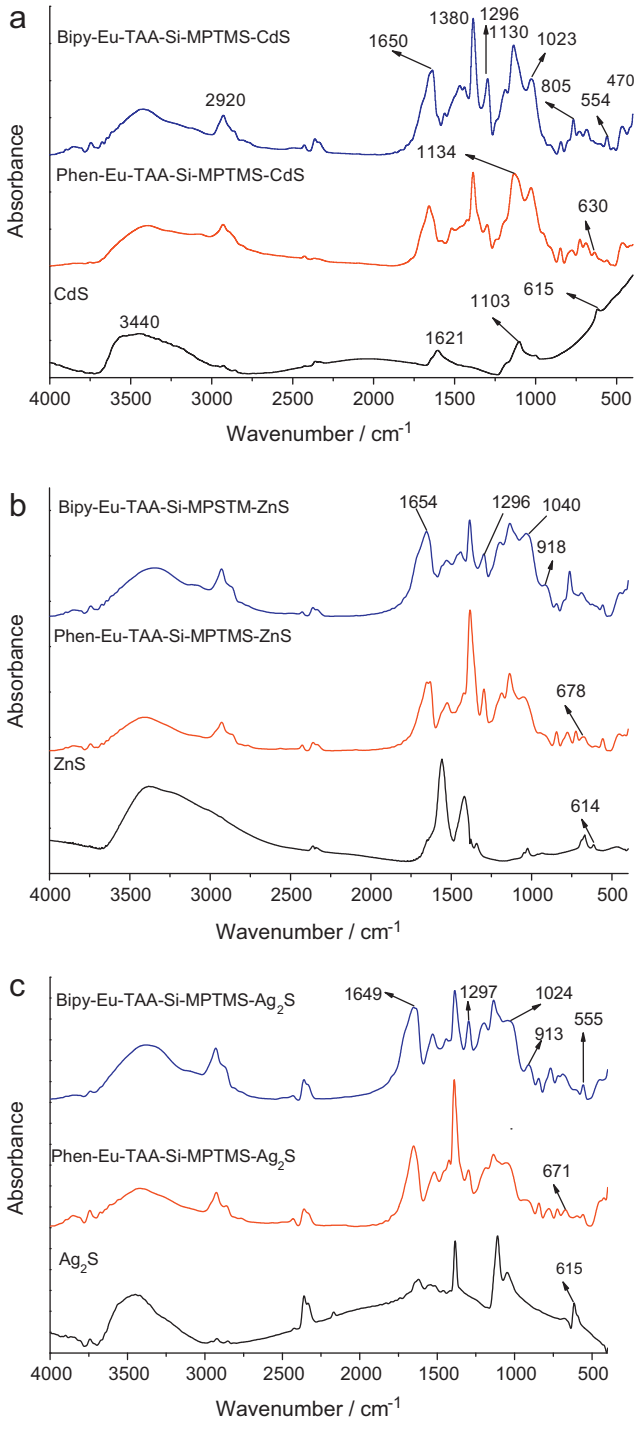

Fig. 2. The FTIR spectra for the semiconductor metal sulfides CdS(ZnS, Ag_2S) and the multicomponent hybrids Phen(Bipy)-Eu-TAA–Si–MPTMS–CdS (ZnS, Ag_2S).

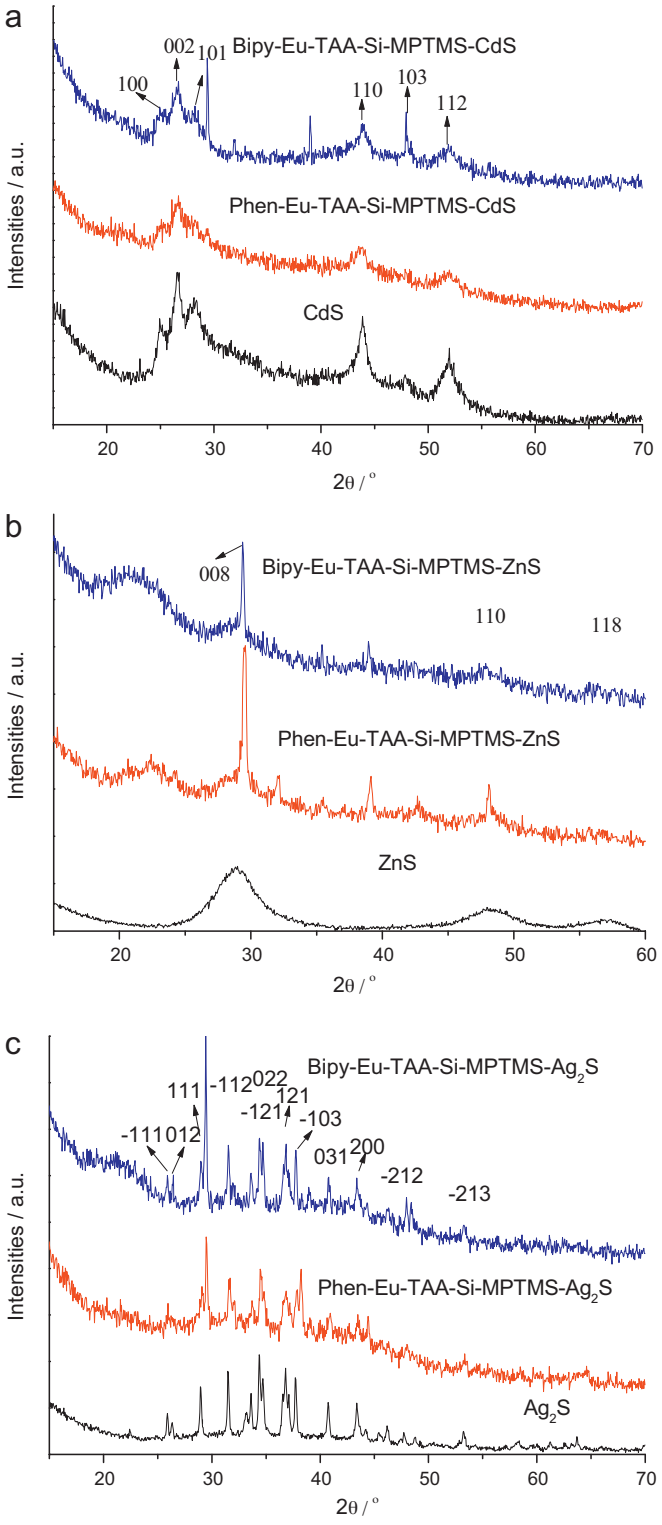

Fig. 3. X-ray diffraction pattern for the semiconductor metal sulfides CdS(ZnS, Ag_2S) and the multicomponent hybrids Phen(Bipy)-Eu-TAA–Si–MPTMS–CdS (ZnS, Ag_2S).

in the IR spectra of the hybrids, which reveals that the S–H group of MPTMS unit is destroyed and are modified to CdS [35]. Furthermore, the peak at 1650 cm^{-1} is originated from –CONH– group of the modified organic ligands [36]. The apparent band at 1380 cm^{-1} can be checked, which belongs to the characteristics of NO_3^- and the Phen or Bipy group [37]. The low frequency at around 470 cm^{-1} verifies that the Eu–O coordination. Fig. 2(b) and (c) shows the identical features as Fig. 2(a) for the only difference of semiconductor metal sulfide unit.

Fig. 3(a) displays the XRD pattern of the initial CdS nanoparticles at room-temperature, which is mostly consistent with JCPDS card (41-1049). All the diffraction peaks are indexed to be the hexagonal phase α-CdS with wurtzite structure, and not the mixed diffraction peaks of Cd, CdO. There exist three peaks at about 25°, 26.5°, and 28.5°, respectively, corresponding to (1 0 0), (0 0 2), and (1 0 1) planes and another three peaks at 44°, 48°, and 52° for the (1 1 0), (1 0 3), and (1 1 2) planes, respectively. When the organically modified Si–O network is assembled with CdS, the XRD pattern

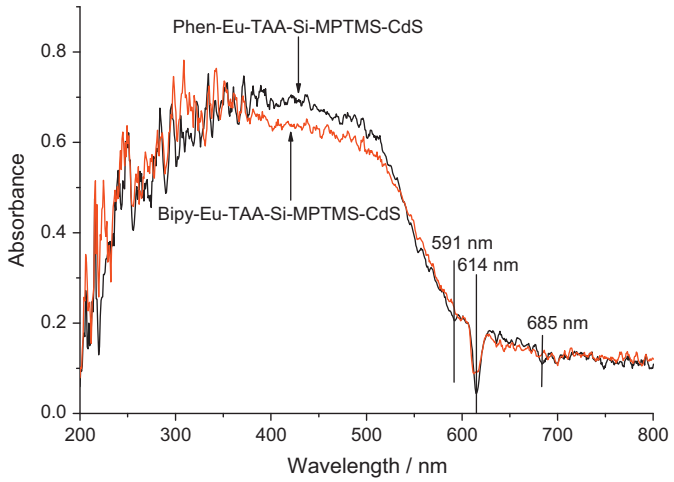

Fig. 4. Selected ultraviolet–visible diffuse reflection absorption spectra of Phen-Eu-TAA–Si–MPTMS–CdS and Bipy-Eu-TAA–Si–MPTMS–CdS.

cannot be changed apparently except for the diffraction peak intensity of them becomes slightly weak, which is due to the fact that the content of CdS is decreased within the whole multicomponent hybrid system and the whole crystalline state also decreases. For Fig. 3(b) on ZnS based system, the peaks at about 28°, 47°, and 56° curves show similar broad peaks around 21°, which is typically caused by amorphous silica materials and this result indicates the existence of the component of SiO_2. Besides, the peaks at about 28°, 47°, and 56° in the figure can be attributed to hexagonal wurtzite-8H ZnS. Moreover, the narrow peaks in the XRD pattern can be due to the incompleteness of hydrolysis-condensation reactions. The XRD patterns of the final hybrid materials Phen-Eu-TAASi–SiO_2–MPTMS–SiO_2/CdS are shown in Fig. 3(b) and (c). Furthermore, none of the hybrid materials contains measurable amounts of phases corresponding to the pure organic compound or free europium nitrate, which is an initial indication for the formation of the true covalent-bonded molecular hybrid materials. On the other hand, highly crystalline Ag_2S is found when the precursor molecules are injected at 160 °C as confirmed by a series of Bragg reflections that correspond to the standard monoclinic R-phase ($P21/c$) of Ag_2S (JCPDS14-72). Fig. 3(c) shows the XRD patterns of Ag_2S and the corresponding hybrid materials. All the peaks can be indexed as the pure monoclinic phase Ag_2S without any impurity. The XRD patterns of two hybrids show the feature peaks of Ag_2S with low crystalline state and weak intensity. From the XRD patterns, it can be concluded that the multicomponent hybrid systems keep the crystalline state of semiconductor metal sulfides whose crystalline framework is beneficial for the whole hybrids to from the amorphous state to crystalline state.

Diffuse reflectance experiments are performed for all the powdered materials and Fig. 4 shows the selected diffuse absorption spectra of Phen(Bipy)-Eu-TAASi–SiO_2–MPTMS–CdS hybrids. Both of the spectra exhibit the similar broad absorption band in the UV–VIS range (200–600 nm), which can be attributed to the absorption of the double cross-linking siloxane (TTASi–MPTMS) derived CdS (Si–O) network. The ligands' $\pi \rightarrow \pi^*$ absorption of Phen or Bipy may be covered by wide absorption of Si–O host and cannot be identified. It is worthy pointing out that the absorption side can be extended to so wide as 600 nm in visible bands, which may be mainly due to the exist of CdS framework in the hybrid system. The other hybrids display the similar character.

The selected scanning electron micrographs (SEM) for the hybrids Phen-Eu-TAASi–SiO_2–MPTMS–CdS(ZnS, Ag_2S) exhibit that the molecular-based material is obtained via a sol–gel process that are shown in Fig. 5 with different metal sulfide

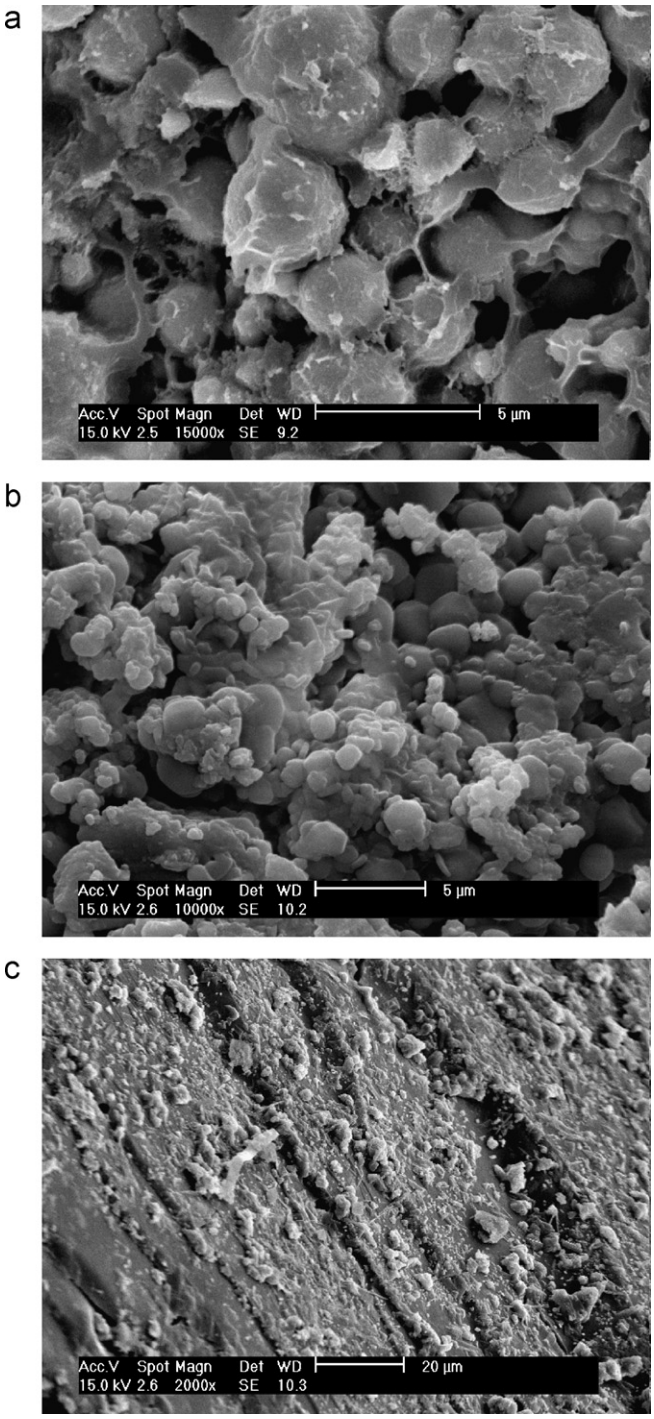

Fig. 5. SEM images of the hybrid materials Phen-Eu-TAA–Si–MPTMS–CdS (ZnS, Ag_2S).

frameworks (a–c). The scanning electron micrographs for the hybrid materials demonstrate that a complicated huge molecular network is formed via a self-assembly process during the hydrolysis/polycondensation process so that the inorganic and organic phases can exhibit their distinct properties together. The reason is speculated that the covalent-bonding (Si–O–Si) enhanced the miscibility of the organic compounds and the silica matrices. What attracted us most is that the spherical particles can be gathered together, which forms the final structure as we have seen in the micrographs. From Fig. 5(a) and (b) we can see that the SEM images of Phen-Eu-TAASi–SiO_2–MPTMS–CdS(ZnS) are both

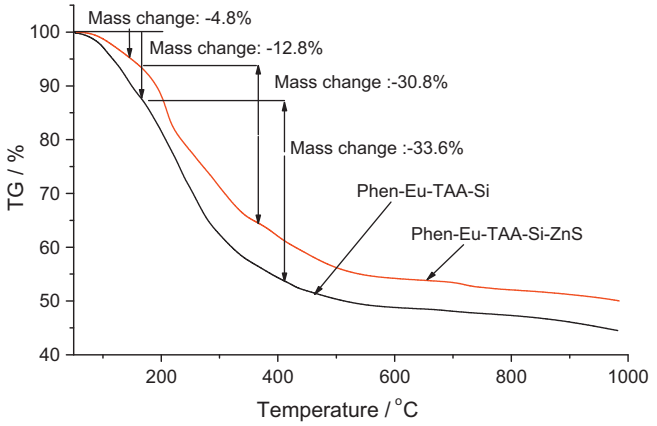

Fig. 6. Selected TG curves of Phen-Eu-TAA–Si and Bipy-Eu-TAA–Si–MPTMS–ZnS hybrids.

sphere-like particle. This can be easily understood for CdS and ZnS possesses the similar crystal structure. The particle size of Phen-Eu-TAASi–SiO_2–MPTMS–CdS (about 2–3 μm) is larger than that of Phen-Eu-TAASi–SiO_2–MPTMS–ZnS (about 0.5–1.0 μm). The only distinction of the two hybrids is the CdS and ZnS, suggesting that metal sulfide framework can have influence on the growth process of hybrids (cohydrolysis and copolycondensation process) through the MPTMS–CdS (or MPTMS–ZnS). Fig. 5(c) for Phen-Eu-TAASi–SiO_2–MPTMS–Ag_2S hybrids are different from the above two hybrids, which does not show apparent sphere-like morphology. The crystal structure of Ag_2S is very different from CdS and ZnS, so the difference of inorganic sulfide framework affects the different morphology.

The selected thermogravimetric weight loss curves of hybrids Phen-Eu-TAA–Si and Phen-Eu-TAASi–SiO_2–MPTMS–ZnS are given in Fig. 6. Comparing the two curves, it can be observed that the hybrid materials with ZnS framework show a slightly stronger thermal stability than the hybrids without ZnS. Both the water loss temperature and the decomposition temperature of organic groups for Phen-Eu-TAASi–SiO_2–MPTMS–ZnS show increase. For Phen-Eu-TAA–Si hybrids, three main thermal weight loss processes can be found. The first is at 84 °C with thermal weight loss of 2.8%, corresponding to the dehydrate process. The second takes place at 180 °C with thermal weight loss of 33.6%, which is originated to the thermal decomposition of organic TTASi and MPTMS groups. The last is the thermal decomposition of Phen with weight loss of 8.4% at 385 °C. While for Phen-Eu-TAASi–SiO_2–MPTMS–ZnS hybrids, there exist three weight loss processes as well. The dehydrate process begins at 165 °C with thermal weight loss of 6.3%. The first thermal decomposition process occurs at 241 °C with thermal weight loss of 30.6%, which is originated to the thermal decomposition of organic TTASi and MPTMS groups. The last is the thermal decomposition of Phen with weight loss of 6.9% at 440 °C. It is found that the introduction of ZnS has an apparent influence on the thermal stability of the whole hybrid system, which is mainly due to the crystal state framework nature of ZnS. In addition, comparing to the two curves, the difference of the weight loss between Phen-Eu-TAA–Si and Phen-Eu-TTASi–SiO_2–MPTMS–ZnS seems to be 10% at 1000 °C. From the TG study, the amount of the semiconductor particle can be approximately 10% in weight. In the experiment, the amount of ZnS in the whole hybrid system is adopted with the molar ratio of Zn(ZnS):S(MPTMS) = 1:1. According to molar ratio, in the final hybrids, the weight ratio of ZnS can be estimated to be around 8%, which is approximately close to the 10% weight loss in the TG curves.

Figs. 7–9 shows the excitation and emission spectra of europium hybrid materials with three semiconductor sulfides. Both excitation

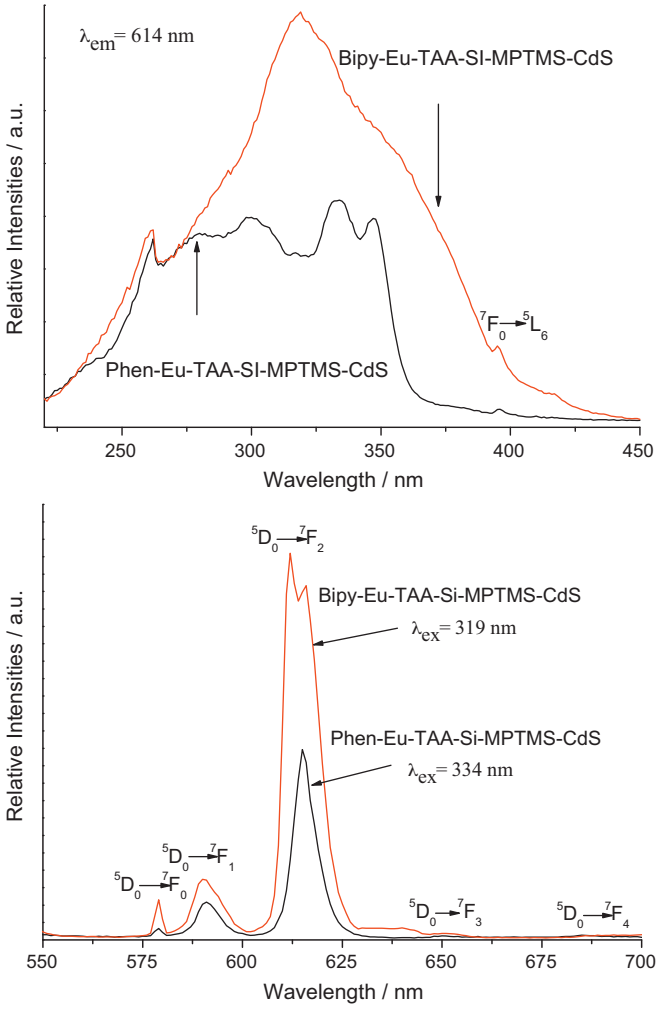

Fig. 7. The excitation and emission spectra of the hybrid materials Phen-Eu-TAA–Si–MPTMS–CdS and Bipy-Eu-TAA–Si–MPTMS–CdS.

and emission show the similar feature to the hybrids without metal sulfides (see Fig. 10), whose excitation is mainly originated from the TTA modified Si–O network (involving Phen or Bipy) and emission is the characteristic transition of Eu^{3+}. The excitation spectra for the europium hybrid materials are obtained by monitoring the emission of Eu^{3+} ions at 614 nm and dominated by broad absorption peaks located at 220–400 nm in the ultraviolet region, which are attributed to double cross-linking siloxane (TTASi–MPTMS) derived ZnS(CdS, Ag_2S) network. The excitation band of the $\pi \rightarrow \pi^*$ electron transition of the ligands (Phen or Bipy) can also be found at the short wavelength of 265 nm clearly. Besides, the apparent absorption of semiconductor sulfide (CdS, ZnS, Ag_2S) cannot be identified separately, it can predicted that the split excitation peak (200–350 nm) in the broad bands may be related to the absorption of them and overlapped with the absorption of organically bonded Si–O network. Certainly, the charge transfer state occurring around 250 nm and 300 nm can also be included in the wide excitation bands. This suggests that the main energy donor in the hybrid system may be the double cross-linking siloxane (TAASi–MPTMS) derived SiO_2/ZnS (Si–O) network and the organic ligand Phen or Bipy. The other weak narrow line locates at 397 nm is attributed to the strongest $^7F_0 \rightarrow {}^5L_6$ transition of Eu^{3+} [38]. So here it can be seen that the semiconductor metal sulfides play the main rigid crystalline framework in the whole hybrid system and the role is not obvious in the photophysical process.

Table 1
Luminescence efficiencies and lifetimes for the europium hybrid materials.

Hybrids	I_{02}/I_{01}	τ (ms)	$1/\tau$ (s^{-1})	A_{rad} (s^{-1})	A_{nrad} (s^{-1})	η (%)
Phen-Eu-TAA–Si	7.7	0.71	1408	420	988	30
Bipy-Eu-TAA–Si	7.4	0.63	1587	408	1179	26
Phen-Eu-TAASi–SiO_2–MPTMS–CdS	7.0	0.64	1562	320	1242	25
Bipy-Eu-TAASi–SiO_2–MPTMS–CdS	9.1	0.63	1587	490	1097	31
Phen-Eu-TAASi–SiO_2–MPTMS–ZnS	8.8	0.79	1266	506	760	40
Bipy-Eu-TAASi–SiO_2–MPTMS–ZnS	7.5	0.61	1639	328	1311	20
Phen-Eu-TAASi–SiO_2–MPTMS–Ag_2S	7.9	0.66	1515	431	1084	29
Bipy-Eu-TAASi–SiO_2–MPTMS–Ag_2S	7.4	0.63	1587	574	1013	36

The corresponding emission spectra show the characteristic luminescence of Eu^{3+} ions using the maximum excitation peak as the excitation wavelength. The five emission lines are assigned to the $^5D_0 \rightarrow {}^7F_0$, $^5D_0 \rightarrow {}^7F_1$, $^5D_0 \rightarrow {}^7F_2$, $^5D_0 \rightarrow {}^7F_3$, $^5D_0 \rightarrow {}^7F_4$ transitions at 582, 591, 616–618, 650 and 688 nm, respectively, for europium ion (Figs. 6–8). The $^5D_0 \rightarrow {}^7F_2$ emission around 616–618 nm is the most predominant transition. It is well known that the $^5D_0 \rightarrow {}^7F_2$ transition is a typical electric dipole transition and strongly varies with the local symmetry of Eu^{3+}, while the $^5D_0 \rightarrow {}^7F_1$ transition corresponds to a parity-allowed magnetic dipole transition, which is independent of the host material. Among these transitions, the $^5D_0 \rightarrow {}^7F_2$ transition shows the strongest emission, suggesting that the chemical environment around Eu^{3+} ions is in low symmetry [39]. The strong red luminescence of these multicomponent hybrid materials Phen(Bipy)-Eu-TAASi–SiO_2–MPTMS–CdS(ZnS, Ag_2S) is observed in the emission spectra, which indicates that the effective energy transfer took place from the TAA organically modified Si–O (and Phen(Bipy)) to the chelated Eu^{3+}. Moreover, the intensity ratios of the luminescent transitions ($^5D_0 \rightarrow {}^7F_2/{}^5D_0 \rightarrow {}^7F_1$) for europium hybrid materials are listed in Table 1. The intensity (the integration of the luminescent band) ratio of the $^5D_0 \rightarrow {}^7F_2$ transition to $^5D_0 \rightarrow {}^7F_1$ transition has been widely used as an indicator of Eu^{3+} site symmetry [40]. When the interactions of the europium complex with its local chemical environment are stronger, the complex becomes more nonsymmetrical and the intensity of the electric-dipolar transitions becomes more intense. As a result, $^5D_0 \rightarrow {}^7F_1$ transition (magnetic dipolar transitions) decreases and $^5D_0 \rightarrow {}^7F_2$ transition (electric-dipolar transitions) increases. The intensity ratios of ($^5D_0 \rightarrow {}^7F_2/{}^5D_0 \rightarrow {}^7F_1$) ($I_{02}/I_{01}$, red/orange) for these multicomponent hybrids have not shown apparent difference (7.0–9.1), suggesting the similar environment surrounding

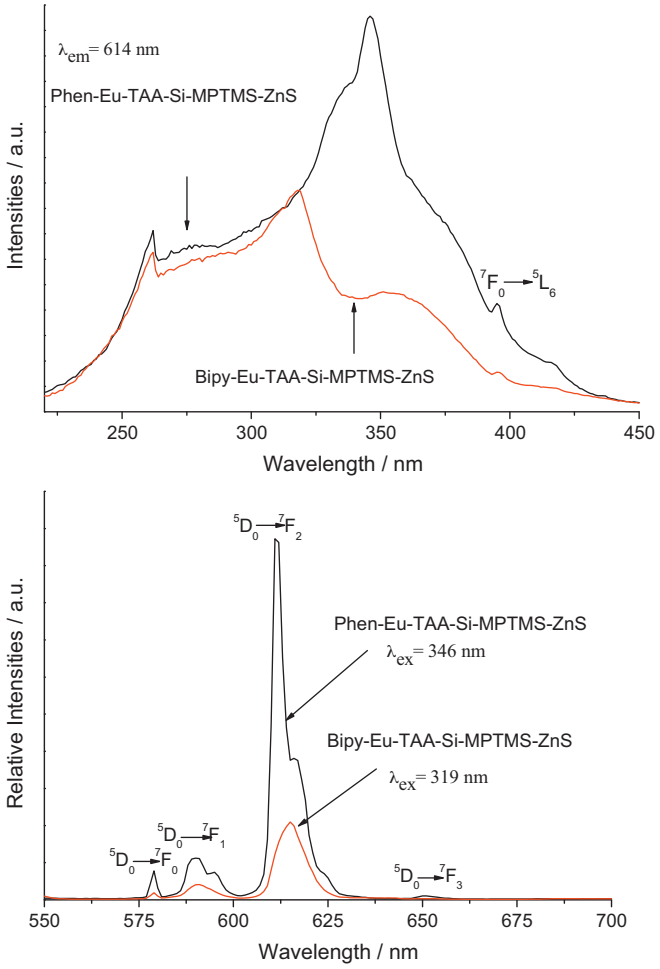

Fig. 8. The emission spectra of the hybrid materials Phen-Eu-TAA–Si–MPTMS–ZnS and Bipy-Eu-TAA–Si–MPTMS–ZnS.

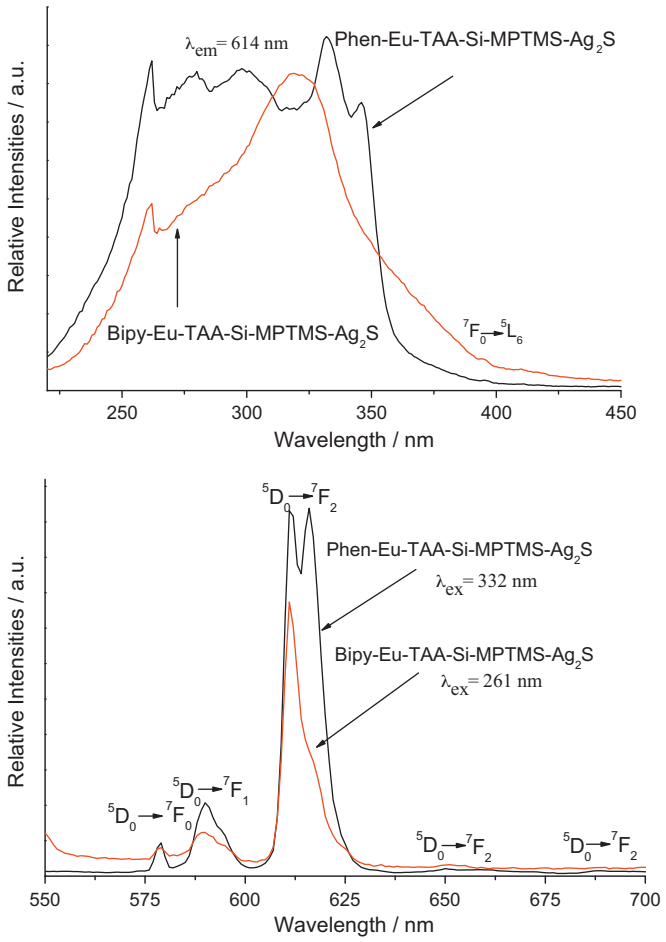

Fig. 9. The emission spectra of the hybrid materials Phen-Eu-TAA–Si–MPTMS–Ag_2S and Bipy-Eu-TAA–Si–MPTMS–Ag_2S.

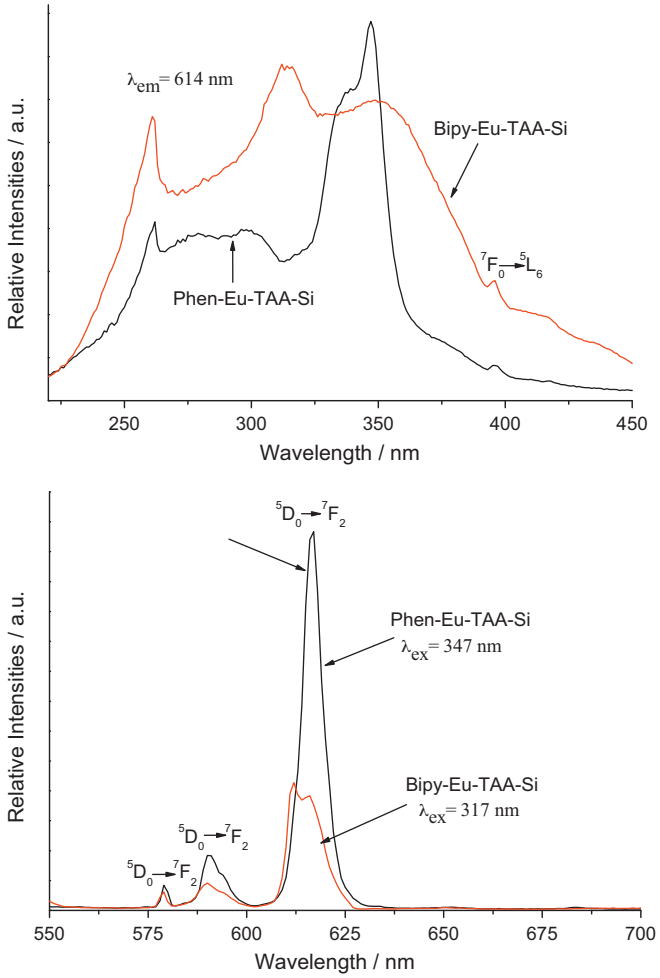

Fig. 10. The emission spectra of the hybrid materials Phen-Eu-TAA–Si and Bipy-Eu-TAA–Si.

Eu^{3+} within the hybrid system (see Table 1). This result can be easily understood. The basic coordination environment around Eu^{3+} is the same (six C=O group O atoms from TAASi and two N atoms from Phen or Bipy), so different metal sulfides only can have indirect influence on the Eu^{3+} in the whole hybrid system.

The typical decay curves of the Eu hybrid materials all single exponential, indicating that all Eu^{3+} ions occupy the same average coordination environment (see Table 1). Similar to the R/O intensity ratio, the luminescent lifetimes of these hybrids only show the little difference (considering the experimental error of lifetime ±10%). From the emission spectra and the lifetime (τ) measurements of the Eu^{3+} first excited level (τ, $^5D_0$), the emission quantum efficiency (η) of the $^5D_0$ excited state can be defined as follows [41]:

$$\eta = \frac{A_{rad}}{A_{rad} + A_{nrad}} \quad (1)$$

A_{rad} and A_{nrad} mean to the radiative transition rate and nonradiative transition rate, respectively, among A_{rad} can be determined from the summation of A_{0J} [42,43].

$$A_{rad} = \sum A_{0J} = A_{00} + A_{01} + A_{02} + A_{03} + A_{04} \quad (2)$$

$$A_{0J} = A_{01}\left(\frac{I_{0J}}{I_{01}}\right)\left(\frac{\nu_{01}}{\nu_{0J}}\right) \quad (3)$$

A_{01} is the Einstein's coefficient of spontaneous emission between the $^5D_0$ and $^7F_1$ energy levels, which can be determined to be 50 s^{-1} approximately and as a reference to calculate the value of other A_{0J} [44,45]. I is the emission intensity and can be taken as the integrated intensity of the $^5D_0 \rightarrow {}^7F_J$ emission bands [44,45]. ν_{0J} refers to the energy barrier and can be determined from the emission bands of Eu^{3+}'s $^5D_0 \rightarrow {}^7F_J$ emission transitions.

The nonradiative transition rates can be obtained through the following equation:

$$\tau = (A_{rad} + A_{nrad})^{-1} \quad (4)$$

And then the quantum efficiency can be calculated from the luminescent lifetimes, radiative and nonradiative transition rates.

From the discussion mentioned above, it can be seen that the value η mainly depends on the values of two factors: one is lifetime and the other is I_{02}/I_{01} (red/orange ratio). If the lifetimes and red/orange ratio are large, the quantum efficiency must be high. As shown in Table 1 all these hybrids show the luminescent efficiency at the range of 20–40% with the same order. The multicomponent hybrids with metal sulfide framework still keep the similar efficiency value as the hybrids without metal sulfide and especially Phen-Eu-TAASi–SiO_2–MPTMS–ZnS hybrids present the highest luminescent quantum efficiency of 40%. In fact, the introduction of the metal sulfide in the whole hybrid system decreases the effective concentration of Eu^{3+} in the hybrids.

4. Conclusions

In summary, we have prepared three series of novel luminescent multicomponent organic–inorganic hybrid materials (Phen(Bipy)-RE-TTASi–SiO_2–MPTMS–SiO_2/CdS(ZnS, Ag_2S)) using double cross-linking siloxane TESPIC–MPTMS as a covalent linkage which can both coordinate to Eu^{3+} and form an inorganic Si–O–Si network though a sol–gel process. The diffraction patterns of them indicate that the metal sulfide semiconductors provide the crystalline state framework for the whole hybrid system and can be connected with the organic parts. The photoluminescent behaviors of these hybrids are studied in detail, which suggest that the introduction of metal sulfides can still maintain the matched luminescent lifetimes and quantum efficiencies in spite of the decreasing concentration of Eu^{3+}.

Acknowledgements

This work is supported by the National Natural Science Foundation of China (20971100), the program for New Century Excellent Talents in University (NCET-08-0398) and the Developing Science Fund of Tongji University.

Appendix A. Supplementary data

Supplementary data associated with this article can be found, in the online version, at doi:10.1016/j.jphotochem.2011.07.010.

References

[1] J. Silver, R. Withnall, Probes of structural and electronic environments of phosphor activators: Mossbauer and Raman spectroscopy, Chem. Rev. 104 (2004) 2833–2855.
[2] J. Kido, Y. Okamoto, Organo lanthanide metal complexes for electroluminescent materials, Chem. Rev. 102 (2002) 2357–2368.
[3] Z.G. Chen, H.L. Chen, H. Hu, M.X. Yu, F.Y. Li, Q. Zhang, Z.G. Zhou, T. Yi, C.H. Huang, Versatile synthesis strategy for carboxylic acid-functionalized upconverting nanophosphors as biological labels, J. Am. Chem. Soc. 130 (2008) 3023–3029.
[4] G. Blasse, B.C. Grabmaier, Luminescent Materials, Springer-Verlag Telos, 1994.
[5] R.C. Ropp, Luminescence and the Solid State, 2nd edition, Elsevier Science, 2004.
[6] A. Kitai, Luminescent Materials and Applications, Wiley, 2008.
[7] T. Justel, H. Nikol, C. Ronda, New developments in the field of luminescent materials for lighting and displays, Angew. Chem. Int. Ed. 37 (1998) 3085–3103.
[8] S.V. Eliseeva, J.C.G. Bunzli, Lanthanide luminescence for functional materials and bio-sciences, Chem. Soc. Rev. 39 (2010) 189–227.

[9] L.R. Matthews, E.T. Knobbe, Luminescence behavior of europium complexes in sol–gel derived host materials, Chem. Mater. 5 (1993) 1697–1700.
[10] A.M. Klonkowski, S. Lis, M. Pietraszkiewicz, Z. Hnatejko, K. Czarnobaj, M. Elbanowski, Luminescence properties of materials with Eu(III) complexes: role of ligand, coligand, anion, and matrix, Chem. Mater. 15 (2003) 656–663.
[11] C. Sanchez, F. Ribot, Design of hybrid organic–inorganic materials synthesized via sol–gel chemistry, New J. Chem. 18 (1994) 1007–1047.
[12] C.X. Du, L. Ma, Y. Xu, W.L. Li, Synthesis and fluorescent properties of europium–polymer complexes containing naphthoate and 1,10-phenanthroline ligands, J. Appl. Polym. Sci. 66 (1997) 1405–1410.
[13] P. Lenaerts, A. Storms, J. Mullens, J. D'Haen, C. Gorller-Walrand, K. Binnemans, K. Driesen, Thin films of highly luminescent rare earth complexes covalently linked to an organic–inorganic hybrid material via 2-substituted imidazo(4,5-f)-1,10-phenanthroline groups, Chem. Mater. 17 (2005) 5194–5201.
[14] L.D. Carlos, R.A.S. Ferreira, V.D. Bermudez, S.J.L. Ribeiro, Lanthanide-containing light-emitting organic–inorganic hybrids: a bet on the future, Adv. Mater. 21 (2009) 509–534.
[15] K. Binnemans, Lanthanide-based luminescent hybrid materials, Chem. Rev. 109 (2009) 4283–4374.
[16] S. Gupta, W.E. Fenwick, A. Melton, MOVPE growth of transition-metal-doped GaN and ZnO for spintronic applications, in: 14th International Conference on Metal Organic Vapor Phase Epitaxy, June 01–06, J. Cryst. Growth 310 (2008) 5032–5038.
[17] N. Manyala, J.F. DiTusa, G. Aeppli, A.P. Ramirez, Doping a semiconductor to create an unconventional metal, Nature 454 (2008) 976–980.
[18] W.H. Chang, C.H. Lee, Y.C. Chang, Nanometer-thick single-crystal hexagonal Gd_2O_3 on GaN for advanced complementary metal-oxide-semiconductor technology, Adv. Mater. 21 (2009) 4970–4972.
[19] A.N. Nazarov, S.I. Tiagulskyi, I.P. Tyagulskyy, The effect of rare-earth clustering on charge trapping and electroluminescence in rare-earth implanted metal-oxide-semiconductor light-emitting devices, J. Appl. Phys. 107 (2010) 123112.
[20] M.M. Mezdrogina, V.V. Krivolapchuk, Y.V. Kozhanova, Spatial distribution of defects and the kinetics of nonequilibrium charge carriers in GaN wurtzite crystals doped with Sm, Eu, Er, Tm, and supplementary Zn impurities, Semiconductors 42 (2008) 159–172.
[21] N. Nepal, J.M. Zavada, D.S. Lee, A.J. Steckl, A. Sedhain, J.Y. Lin, H.X. Jiang, Deep ultraviolet photoluminescence of Tm-doped AlGaN alloys, Appl. Phys. Lett. 94 (2009) 111103.
[22] R. Martin, Visible luminescent RE-doped GaN, AlGaN and AlIn. In rare earth doped III-nitrides for optoelectronic and spintronic application, Top. Appl. Phys. 124 (2010) 189–219.
[23] Y.S. Liu, W.Q. Luo, R.F. Li, G.K. Liu, M.R. Antonio, X.Y. Chen, Optical spectroscopy of Eu^{3+} doped ZnO nanocrystals, J. Phys. Chem. C 112 (2008) 686–694.
[24] Y.P. Du, Y.W. Zhang, L.D. Sun, C.H. Yan, Efficient energy transfer in monodisperse Eu-doped ZnO nanocrystals synthesized from metal acetylacetonates in high-boiling solvents, J. Phys. Chem. C 112 (2008) 12234–12241.
[25] J.J. Li, G.M. Xu, Preparation and applications of doped ZnS nanoparticles, Prog. Chem. 22 (2010) 861–866.
[26] S.L. Ji,.L. Yin, G.D. Liu, L.D. Zhang, C.H. Ye, Synthesis of rare earth ions-doped ZnO nanostructures with efficient host–guest energy transfer, J. Phys. Chem. C 113 (2009) 16439–16444.
[27] W.Q. Luo, R.F. Li, G.K. Liu, M.R. Antonio, R. Mark, X.Y. Chen, Evidence of trivalent europium incorporated in anatase TiO_2 nanocrystals with multiple sites, J. Phys. Chem. C 12 (2008) 10370–10377.
[28] J. del-Castillo, A.C. Yanes, J. Mendez-Ramos, Undoped and Eu^{3+} doped In_2O_3 quantum-Ddots in transparent glass-ceramics, J. Nanosci. Nanotechnol. 9 (2009) 4834–4838.
[29] C. Louis, S. Roux, G. Ledoux, C. Dujardin, O. Tillement, B.L. Cheng, P. Perriat, Luminescence enhancement by energy transfer in core–shell structures, Chem. Phys. Lett. 42 (2006) 157–160.
[30] G. Jose, C. Joseph, Cyriac, M.A. Ittyachen, N.V. Unnikrishnan, Structural and optical characterization of CdSe nanocrystallites/rare earth ions in sol–gel glasses, Opt. Mater. 29 (2007) 1495–1500.
[31] Y.J. Li, B. Yan, Photophysical properties of a novel organic–inorganic hybrid material: Eu(III)-β-diketone complex covalently bonded to SiO2/ZnO composite matrix, Photochem. Photobiol. 86 (2010) 1008–1015.
[32] B. Yan, Y. Zhao, Y.J. Li, Novel photofunctional multicomponent rare earth (Eu^{3+}, Tb^{3+}, Sm^{3+} and Dy^{3+}) hybrids with double cross-linking siloxane covalently bonding SiO_2/ZnS nanocomposite, Photochem. Photobiol. 87 (2011) 757–765.
[33] B. Yan, C. Wang, L. Guo, J.L. Liu, Photophysical properties of Eu(III) center covalently immobilized in Si–O–B and Si–O–Ti composite gels, Photochem. Photobiol. 86 (2010) 499–506.
[34] M.C. Goncalves, V.D. Bermudez, R.A.S. Ferreira, L.D. Carlos, D. Ostrovskii, J. Rocha, Optically functional diurethanesil nanohybrid gel containing Eu^{3+} ions, Chem. Mater. 16 (2004) 2530–2543.
[35] F.H. Huang, Synthesis and spectral properties of cuboid-shaped CdS particles, Spectrosc. Spect. Anal. 28 (2008) l03–l105.
[36] H.R. Li, J. Lin, H.J. Zhang, L.S. Fu, Q.G. Meng, S.B. Wang, Preparation and luminescence properties of hybrid materials containing europium(III) complexes covalently bonded to a silica matrix, Chem. Mater. 14 (2002) 3651–3655.
[37] K. Nakamoto, Infrared and Raman Spectra of Inorganic and Coordination Compounds. Part B. Applications in Coordination, Organometallic, and Bioinorganic Chemistry, 6th edition, Wiley-Interscience, New York, 2009.
[38] M.D. Regulacio, M.H. Pablico, J.A. Vasquez, P.N. Myers, S. Gentry, M. Prushan, S.W. Tam-Changand, S.L. Stoll, Luminescence of Ln(III) dithiocarbamate complexes (Ln) La, Pr, Sm, Eu, Gd, Tb, Dy, Inorg. Chem. 47 (2008) 1512–1523.
[39] K. Binnemans, K. Van Herck, C. Gorller-Walrand, Influence of dipicolinate ligands on the spectroscopic properties of europium(III) in solution, Chem. Phys. Lett. 266 (1997) 297–302.
[40] Z. Wang, J. Wang, H.J. Zhang, Luminescent sol–gel thin films based on europium-substituted heteropolytungstates, Mater. Chem. Phys. 87 (2004) 44–48.
[41] E.E.S. Teotonio, J.G.P. Espinola, H.F. Brito, O.L. Malta, S.F. Oliveria, D.L.A. de Foria, C.M.S. Izumi, Influence of the N-[methylpyridyl]acetamide ligands on the photoluminescent properties of Eu(III)-perchlorate complexes, Polyhedron 21 (2002) 1837–1844.
[42] M.H.V. Werts, R.T.F. Jukes, J.W. Verhoeven, The emission spectrum and the radiative lifetime of Eu^{3+} in luminescent rare earth complexes, Phys. Chem. Chem. Phys. 4 (2002) 1542–1548.
[43] O.L. Malta, H.F. Brito, J.F.S. Menezes, Spectroscopic properties of a new light-converting device Eu(thenoyltrifluoroacetonate)$_3$ 2(dibenzyl sulfoxide). A theoretical analysis based on structural data obtained from a sparkle model, J. Lumin. 75 (1997) 255–268.
[44] P.C.R. Soares-Santos, H.I.S. Nogueira, V. Félix, Novel rare earth luminescent materials based on complexes of 3-hydroxypicolinic acid and silica nanoparticles, Chem. Mater. 15 (2003) 100–108.
[45] L.D. Carlos, Y. Messaddeq, H.F. Brito, R.A.S. Ferreira, Full-color phosphors from europium(III)-based organosilicates, Adv. Mater. 12 (2000) 594–598.